UNIVERSIDADE ESTADUAL PAULISTA
“JULIO DE MESQUITA FILHO”
INSTITUTO DE GEOCIÊNCIAS E CIÊNCIAS EXATAS

Graduation Final Work

Graduation in Geography

MAPPING OF THE SPATIAL DISTRIBUTION AND TEMPORAL VARIATION OF RUPESTRIAN VEGETATION IN SERRA DO CIPÓ (MG) THROUGH IMAGES OBTAINED BY REMOTELY PILOTED AIRCRAFT

Thais Pereira de Medeiros

Profa. Dra. Leonor Patrícia Cerdeira Morellato (advisor)

Rio Claro (SP)

2019

UNIVERSIDADE ESTADUAL PAULISTA
Instituto de Geociências e Ciências Exatas
Campus of Rio Claro

THAIS PEREIRA DE MEDEIROS

MAPPING OF THE SPATIAL DISTRIBUTION AND TEMPORAL VARIATION OF RUPESTRIAN VEGETATION IN SERRA DO CIPÓ (MG) THROUGH IMAGES OBTAINED BY REMOTELY PILOTED AIRCRAFT

Graduation Work presented to *Instituto de Geociências e Ciências Exatas* - Campus of Rio Claro, of the *Universidade Estadual Paulista Júlio de Mesquita Filho,* to obtain the Bachelor of Geography degree.

Rio Claro - SP
2019

THAIS PEREIRA DE MEDEIROS

MAPPING OF THE SPATIAL DISTRIBUTION AND TEMPORAL VARIATION OF RUPESTRIAN VEGETATION IN SERRA DO CIPÓ (MG) THROUGH IMAGES OBTAINED BY REMOTELY PILOTED AIRCRAFT

Graduation Work presented to *Instituto de Geociências e Ciências Exatas* - Campus of Rio Claro, of the *Universidade Estadual Paulista Júlio de Mesquita Filho*, to obtain the Bachelor of Geography degree.

Examining Committee

Profa. Dra. Leonor Patrícia Cerdeira Morellato (advisor)

Profa. Dra. Cenira Maria Lupinacci

Prof. Dr. Sérgio dos Anjos Ferreira Pinto

Rio Claro, 16 of October of 2019.

Student Signature

Advisor Signature

M488m

Medeiros, Thais Pereira de

Mapping of the spatial distribution and temporal variation of rupestrian vegetation in Serra do Cipó (MG) through images obtained by remotely piloted aircraft / Thais Pereira de Medeiros. -- Rio Claro, 2019

55 p. : tabs., fotos, mapas + 1 CD-ROM

Trabalho de conclusão de curso (Bacharelado e licenciatura - Geografia) - Universidade Estadual Paulista (Unesp), Instituto de Geociências e Ciências Exatas, Rio Claro

Orientadora: Leonor Patrícia Cerdeira Morellato

Coorientador: Thiago Sanna Freire Silva

1. Remote Sensing. 2. Unmanned Aerial System. 3. Rupestrian Grassland. 4. Biodiversity. 5. UAS classification method. I. Título.

Sistema de geração automática de fichas catalográficas da Unesp. Biblioteca do Instituto de Geociências e Ciências Exatas, Rio Claro. Dados fornecidos pelo autor(a).

Acknowledgement

First of all, I thank my family for all the emotional, intellectual and financial support. I thank my mom Rita, my dad Donizete and my little sister Júlia. I thank my advisors, Patrícia Morellato and Thiago Sanna for all the knowledge acquired throughout the research development. I thank my best friends, Milhouse and Bequinha, for all companionship and friendship. I thank my friends, members of the EGRIC group, Liz, Higor, Vitória, Pinóquio, Kenny and John, for all the experience lived during these two years of much "*cavernada*". I thank my friends, Manu, Jay, Gabi, Edu e Xu, for all the memories acquired in my graduation. I thank my dog, Balu, for being with me always independent of anything. And finally, I thank FAPESP and CNPQ for their financial support for the development of the research.

Let them fly and they will create a new remote sensing market in your country (COLOMINA; MOLINA, 2014).

Abstract

The Serra do Cipó, located in Cadeia do Espinhaço, north of Belo Horizonte (MG), inside of the domain of the Cerrado and with predominance of phytophysiognomy of rupestrian grassland, is characterized by a high richness and endemicity of herbaceous species. Cadeia do Espinhaço is the center of diversity of various group of plants, including more than 4000 species and, the region of Serra do Cipó, covering approximately 200 kilometers inside of the Espinhaço, shelter more than a third of this biodiversity. These regions are currently under great threat, mainly by tourism activity and mining. Therefore, is extremely important the development of new methods and approaches that allow the effective monitoring of these environments, and so making possible to better understand its operation and vulnerabilities. The Unmanned Aerial Vehicles (UAVs), also known as Remotely Piloted Aircraft (RPAs), are equipments that contribute for the studies and monitoring of both the environmental and ecologic vulnerabilities of such environments. The OBIA (Object Based Image Analysis) classification method has been used successfully for the analysis of high resolution images. However, they still present many difficulties for the automatic classification of surface elements, due to the extremely high spatial resolution of their sensors. The use of these technologies for the monitoring of heterogeneous vegetation in actually is still challenging due to the great structural and spatial heterogeneity existing in these environments. In this context, the goal of the research was answer the following questions: What are the better combinations of parameters for proposing a high quality of ultrahigh spatial resolution classification? Is the OBIA an efficient method for classifying an heterogeneous ecosystem, such as Serra do Cipó? Does the spatial resolution influence species classification? What is the optimal spatial resolution for classifying an image with the ultrahigh spatial resolution?

Key-words: UAS, rupestrian grassland, OBIA method.

Resumo

A Serra do Cipó, localizada na Cadeia do Espinhaço, ao norte de Belo Horizonte (MG), dentro do domínio do Cerrado e com predominância de fisionomia de campos rupestres, é caracterizada por uma alta riqueza e endemicidade de espécies herbáceas. A Cadeia do Espinhaço é o centro de diversidade de vários grupos de plantas, incluindo mais de 4000 espécies e, a região da Serra do Cipó, abrangendo aproximadamente 200 km² dentro do Espinhaço, abriga mais que um terço dessa biodiversidade. Estas regiões encontram-se atualmente sob grande ameaça, principalmente pela atividade turística e pela mineração. Portanto, é de extrema importância o desenvolvimento de novos métodos e abordagens que permitam o monitoramento eficaz destes ambientes, e assim possibilitem uma melhor compreensão de seu funcionamento e vulnerabilidades. Os Veículos Aéreos Não Tripulados (VANTs), também conhecidos como Aeronaves Remotamente Pilotadas (ARP) são equipamentos que contribuem para os estudos e monitoramento das vulnerabilidades ambientais e ecológicas desses ambientes. O método OBIA (Object Based Image Analysis) de classificação tem sido utilizado com sucesso para a realização de análises a partir das imagens de alta resolução. Entretanto, ainda existem dificuldades para a classificação automática de elementos da superfície, em imagens obtidas por VANTs, devido à altíssima resolução espacial de seus sensores. O uso dessas tecnologias para o monitoramento de vegetações heterogêneas na atualidade ainda é desafiador por conta da grande heterogeneidade estrutural e espacial existente nestes ambientes. Neste contexto, o objetivo do trabalho foi responder as seguintes perguntas: Qual a melhor combinação de parâmetros para obtenção de uma alta qualidade na classificação de imagem com altíssima resolução espacial? O método OBIA é eficiente para classificar ecossistemas heterogêneos, como por exemplo, a Serra do Cipó? A resolução especial das imagens apresenta influencia no processo de classificação? Qual é a resolução especial ideal para classificar uma imagem com altíssima resolução espacial?

Palavras-chaves: VANT, campo rupestre, método OBIA.

FIGURE LIST

TABLE LIST

SUMMARY

1. Introduction

Unmanned Aerial Systems (UAS), also known as Unmanned Aerial Vehicles (UAV), Remotely Piloted Aerial System (RPAS) or simply “drones”, have advanced rapidly to satisfy the needs of a demanding spatial data market (COLOMINA; MOLINA, 2013). This development has been a response to the limitations of conventional remote sensing platforms (satellites and piloted aircrafts), such as high-cost, lack of operational flexibility, limited versatility, poor spatial and temporal resolutions, and cloud contamination.

Currently, modern UAS represent one of the main technological evolutions in remote sensing, having emerged with the goal of producing maps and imagery with high-quality resolution, which conventional photogrammetry does not provide (WHITEHEAD; HUGENHOLTZ, 2014). For ecology and environmental sciences, UAS applications have become increasingly relevant, as ecologists and environmental scientists require data collected at appropriate spatial and temporal resolutions that can only be covered by UAS (GOULD, 2000).

Current UAS platforms offer such as high-spatial resolution imaging, temporal resolution flexibility, low-operational cost, minimized human operation, and also increased maneuverability, and safety in adverse weather and dangerous environments, with reduced risk exposure to pilots (NEX; REMONDINO, 2013). Modern applications and uses of UAS’s include mainly agriculture and environmental, surveillance, aerial monitoring for engineering, cultural heritage (archeological) surveying and the ecological monitoring.

There are still several challenges in using this technology, including development appropriate procedures to manage and extract the information from the high volume, high spatial resolution resulting data. These include the use of image classification algorithms, which have to date been mainly deployed to 0.5 to 500 m spatial resolution images, while UAS images are often in the 0.05 to 0.1 m spatial resolution range and thus very challenging for automatic classification of surface features (ANDERSON; GASTON, 2013).

Object Based Image Analysis (OBIA), more specifically Geographic Object Based Image Analysis (GEOBIA), has been an important method for high resolution image classification, having advantages over traditional pixel-based methods. This methods is based on pre-clustering the image pixels into homogeneous objects (regions, clusters), depend on specific

14spectral characteristics (features, e.g. color, texture), as well as shape characteristics (BLASCHKE, 2010).

In general, remote sensing is a valuable technology for investigating species composition (JENSEN, 2006), and UAS imagery, in particular, has been successfully applied in many fine-scale classification studies, because is possible to identify subtle variations in species composition (LALIBERTE; RANGO, 2011). On the other hand, the ultrahigh spatial resolution of imagery provides a detailed information about vegetation features, including shadows, stems, and vegetation gaps, resulting in misclassification (WATTS, AMBROSIA, HINKLEY, 2012). Heterogeneous ecosystems, for instance, rupestrian grasslands, are generally small in size and highly mixed, making it difficult to obtain a unique spectral or textural feature of image objects to be used in the classification model (LU; HE, 2017).

With the goal of test OBIA classification methodology and propose an improvement of the classification method in ultrahigh spatial resolution imagery, we chose a heterogeneous, highly diverse vegetation, the *campo rupestre* (Silveira et al. 2016, Morellato & Silveira 2018) or rupestrian grassland, located at the Serra do Cipó, Minas Gerais, Southeastern Brazil. The *campo rupestre* presents a mosaic of phytophysionomies, indicating a landscape with high spatial, structure and radiometric complexity.

Considering in the advantages and challenges of UAS image, the research sought to answer the following questions: What are the better combinations of parameters for proposing a high quality of ultrahigh spatial resolution classification? Is the OBIA an efficient method for classifying an heterogeneous ecosystem, such as Serra do Cipó? Does the spatial resolution influence species classification? What is the optimal spatial resolution for classifying an image with the ultrahigh spatial resolution?

2. Literature review

2.1. UAS history and literature evolution

The UAS was born in the military context and the mapping potential of these platforms was discovered by groups and researchers in the late 1970's (COLOMINA; MOLINA, 2014). The oldest platforms used for aerial observation were balloons, kites and, rockets. At first, one of the most interesting experiment was made in 1903, using of small cameras mounted on the breasts of pigeons. This method was proposed by Julius Neubronner, apothecary born in 1852 and was known as the pioneer of amateur photograph and film.

In 1916, the Wright brothers constructed an automatic airplane, called Hewitt-Sperry. Wilbur and Orville Wright were American inventors and dedicated their lives to aviation. Other two important evolution in the aviation science happened in 1933 and in 1973. In 1933, The Royal Navy, the United Kingdom's naval force, used the Queen Bee drone for gunnery practice. And in 1973, the drone called USAF Firebees, developed by the Ryan Aeronautical Company, was used in North Vietnam and during the October War, by Israel against Egyptian (Figure 1).

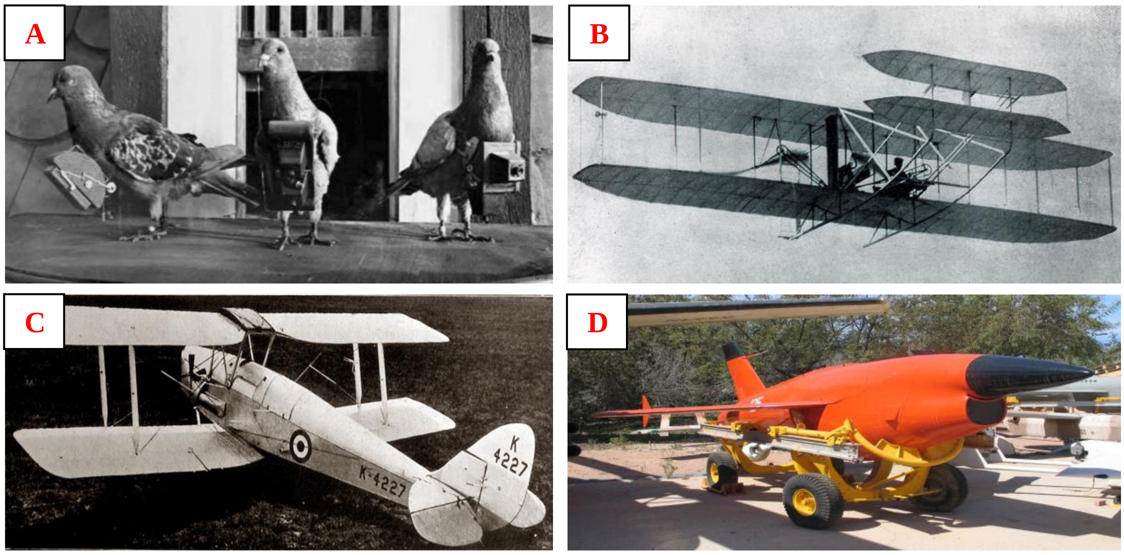

Figure 1: Small camera mounted on the breasts of pigeons, developed by Julius Neubronner (A); Automatic airplane developed by Wright brothers (B); Queen Bee drone developed by Royal Navy (C); USAF Firebees developed by Ryan Aeronautical Company (D).

From the 1970's the UAS development has been a growing up. In 1979, Przybilla and Wester Ebbinghaus tested a radio control and equipped a fixed wing UAS with an optical camera. They dedicated their lives to the study of geomatic and computer vision Sciences. In 1980, a second test was performed by the same team using helicopters model with a premier line of medium format twin lens called "Rolleiflex camera" (WESTER-EBBINGHAUS, 1980) (Figure 2). Over time, navigation and mapping sensors were integrated in the radio controlled platforms with the goal to acquire low-altitude and high-resolution imagery.

Figure 2: Rolleiflex camera: medium format twin lens reflex.

The increase of UAS reports in the literature is clean, because the number of developed UAS has multiplied by three from 2005 to today and a relevant increase is observed in both civil and commercial types of platforms, especially in 2012 and 2013 (COLOMINA, MOLINA, 2014). Since 2009 has shown a clear rise in the use of the term "Drone".

The UAS impact in Science also has been noticeable. For instance, in 2004, the International Society for Photogrammetry and Remote Sensing (ISPRS) received three manuscripts that discussed about UAS; in 2008 the trend changed, the seminar occurred in Beijing obtained 21 manuscripts related to the use of UAS in three different sessions; in 2011 the ISPRS community created a specific conference for UAS, called "UAS-g". These developments impacted conferences and journals of robotics and computer vision. Currently, there is a specific congress about UAS, robotics and computer vision: International Conference on Robotics and Automation (ICRA); International Conference on Intelligent Robots and Systems (IROS), etc.

2.2. Types of UAS

UAS have been classified based on a fixed or a rotary wing. The advantage of fixed wing is the greater speed, longer range, and they launched by hand or a catapult. On the other hand, rotary wing includes miniature helicopters and multirotor platforms, for example, quadcopters (four sets of rotor blades) or octocopters (eight sets of rotor blades), which has shorter flight duration, but offer greater maneuverability. It is important to mention that there are two distinct forms of rotor blades: blades around a central body or the rotors arranged along two arms located on either sides of a payload (Figure 3) (HARDIN; JENSEN, 2011).

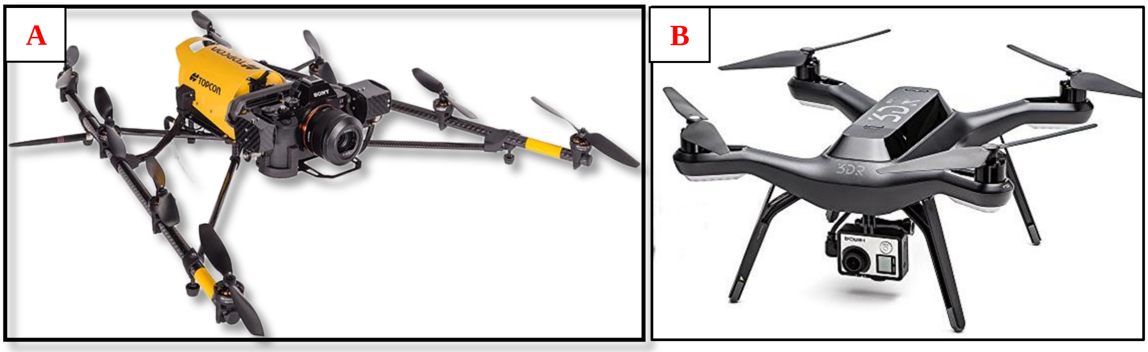

Figure 3: Forms of rotor blades: rotors arranged along two arms located on either sides of a payload (A) and blades around a central body (B).

There are different classifications based on various characteristics of the aerial platforms: size, weight, endurance and aerodynamics; or based on the system operation: nature of its application and mission range or flying altitude (MACKENZIE, 2009). Some scientists created an UAS classification, for example, Eisenbeiss (2009) considers for classifying the UAS some aspects: powered or non-powered platforms, heavier or lighter than air platforms, assessment on range, endurance, weather and wind dependency and maneuverability. Still, Van Blyenburgh (2013) included categorizations based on size, weight, operating range and, certification potential.

The common classification is based on three types: nano, micro, and mini UAS, close, short, and medium range UAS, and the rest of UAS (Table 1). The nano micro mini UAS is characterized by low-weights (less than 30 kilograms), low flying altitude, having less than two hours of flight and less than ten kilometers of range. The close short medium range UAS is characterized by weight between 150 and 1250 kilograms and operating range between 10 and 70 km.

In terms of size and weight terms the UAS is classified in four categories, as can be seen in the table 1:

Size	Characteristics	Payload size
Large	Operation range: more than 500 km; Flight time: two days; Altitude: 3 – 20 km;	200 kg – 900 kg;
Medium	Operation range: 500 km; Flight time: 10 hours; Altitude: up to 4 km;	50 kg;
Small and mini	Operation range: less than 10 km; Flight time: less than one hour; Altitude: up to 1 km;	30 kg – 5 kg;
Micro and nano	Operation range: less than 10 km; Flight time: less than one hour; Altitude: less than 250 m;	Less than 5 kg;

Table 1: The Unmanned aerial system (UAS) classification in four categories based on size and weight of the UAS.

In general, large and medium UAS has been used in military platforms and has a high financial cost because the ground operational is complex, making impractical for most ecological research needs. While, small and mini, micro and nano UAS is characterized by having light-weight, flight time of a few hours, and very limited ranges (Figure 4).

New classes of UAS have been developed: Nano Hummingbird UAV, Mirador Micro UAV, and Phoenix Ornithopters, characterized by highly miniaturized UAS (Table 2 and Figure 5). These systems are still highly experimental and need more development in order to improve their stability operation, but the advantage of these systems aims in lies providing valuable data for ecological studies (MACKENZIE, 2009).

New classes	**Characteristics**
Nano Hummingbird UAV	Weight: 19 grams; Wingspan: 16 cm; Low altitude; Very short flight duration; Can carry a miniaturized video camera;
Mirador Micro UAV	Flight time: 20 minutes; Wingspan: 25 cm; Powered with miniature fuel cells;
Phoenix Ornithopters	Offer more maneuvrability than fixed wing or rotor based microcopters.

Table 2: Three new classes of UAS: nano hummingbird UAV, mirador micro UAV and phoenix ornithopters.

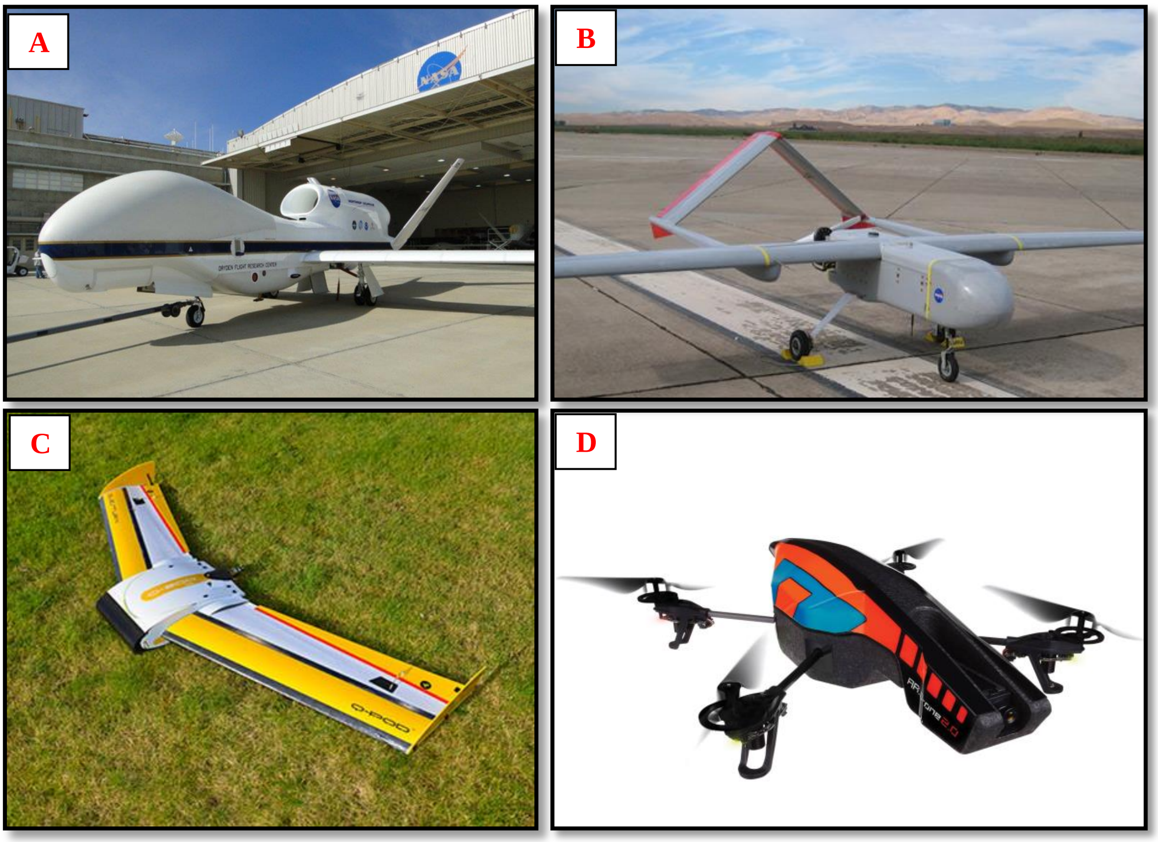

Figure 4: UAS classification based on size, divided in 4 categories: large UAS (A); medium UAS (B); small and mini UAS (C) and micro and nano (D).

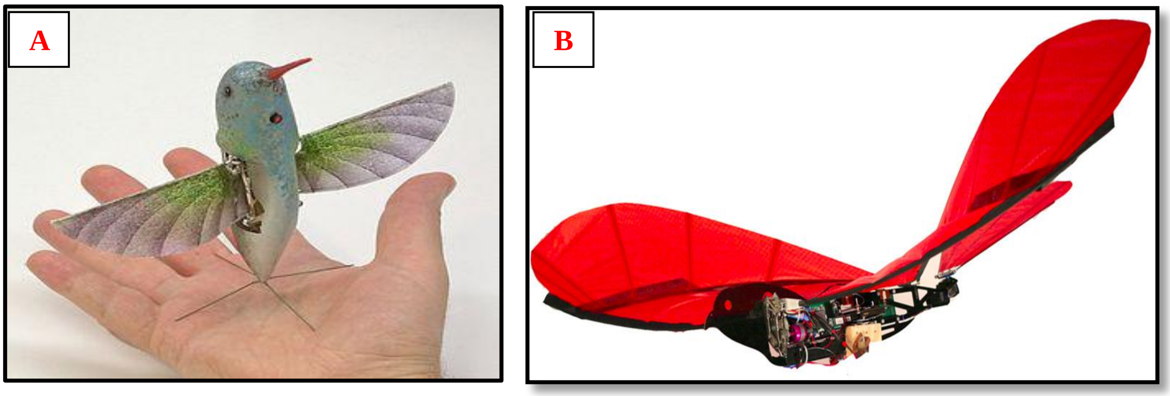

Figure 5: New classes of UAS: Nano Hummingbird UAV (A) and Phoenix Ornithopters (B).

2.3. UAS regulations

The UAS regulations, in general, established three criterias for flight, which includes limited flying altitude, flying within visual range, and proximity to built up areas, and also allow operating an aerial platform with fixed wing or rotary wing less than 30 kilograms; range not greater than 10 km, flying below 300 meters, use small or medium format optical camera within visible spectrum, and use autopilot with Global Navigation Satellite System (GNSS) or Inertial Satellite System (ISS).

Each country have their specific laws and regulations about UAS, for instance, in Canada and United Kingdom it is possible to fly below 400 feet (122 meters) above ground level, but in the United States it is possible to fly below 100 feet (305 meters) above ground level (SFOC TRANSPORT CANADA, 2008).

In 2007, the European Organization for the Safety of Air Navigation, created a document called “Specifications for the Use of Military Remotely Piloted Aircraft (RPA)” dedicated to civil and military uses. In 2009, the European Aviation Safety Agency (EASA) also created a document that established general principles for type certification and environmental protection.

There are some communities and certification about UAS and each one of them dedicated for a specific aspect related to these platforms (EVERAERTS, 2009), which is shown in the following table 3:

Community	Goal
European Defence Agency (EDA)	Traffic insertion; frequency management and future UAS;
Association for Unmanned Vehicle System International (AUVSI)	Advance the unmanned systems and robotic community;
European Organization of Civil Aviation Equipment (EUROCAE)	Aviation standardization;

U.S. Federal Aviation Administration (FAA)	Develop a plan for integrating UAS into the national aircraft system.

Table 3: Communities and certifications about Unmanned Aerial Systems.

Over time, the advanced in regulations were noticeable: in october 2012, the French Civil Aviation Authority made possible civil UAS to fly over 100 kilometers; in December 2012, the private company called “Danish photogrammetric and mapping” authorized the use of UAS for aerial surveys of disasters and in May 2013, the Brazilian National Civil Aviation Agency (*Agência Nacional de Aviação Civil – ANAC*, in portuguese) authorized private operators to fly UAS. It is interesting to say that X-Mobots, a private company situated in São Carlos (São Paulo – Brazil), obtained a Certificate of Experimental Flight Authorization *(Certificado de Autorização de Voo Experimental – CAVE*, in portuguese*).*

2.4. Sensors classification

In traditional remote sensing it is common to use a conventional cameras which covers only the visible region of the spectrum (COLOMINA, MOLINA, 2014). However, this range is limited for some studies and analysis, for example, vegetation. Therefore, new sensors were developed in order to supply this demand.

The main sensors used in UAS are: visible band, near infrared, multispectral, hyperspectral, thermal, lasers scanners, and synthetic aperture radar (VAN BLYENBURGH, 2013). Each one of them is used with a specific goal and has specific characteristics (Table 4).

Sensor	**Characteristic**
Visible band and near infrared	High-quality and low-cost; used with mobile phones (XIE *et al*., 2012);
Multispectral	More expensive, bulkier but presents higher dynamic ranges; Has multiple bands and has adjustable spectral ranges; It is able to discriminate spectral reflectance and is an

	important indicator in applications to study vegetation's health;
Hyperspectral	Extract more detailed information because is able to analyze all channels in the electromagnetic spectrum; Sacrifice spatial resolution for spectral resolution and provides hundreds of spectral bands simultaneously (RUFINO; MOCCIA, 2005);
Thermal	Thermal cameras have a low weight; Suited to the use of low flying aerial platform; It is suited for real time applications, for instance, can identify several thermal hot spots within a test burn (KOSTRZEWA *et al*., 2003); Uses: Forest fire monitoring, monitor the temperature of a number of agricultural tests plots at different times of day, and indicates water uptake by different crops;
Lasers scanners (LiDAR)	It is used for rapid mapping in emergency situations;
Synthetic Aperture Radar (SAR)	SAR has not been much used with UAS, but it is important to generate digital terrain and elevation models in forest areas (REMY *et al*., 2012); One example of synthetic aperture radar is called UASSAR, which was developed by NASA and have been used in a broad range of Science applications – more than 160 flights across the globe.

Table 4: Characteristics of the six types of sensors used coupled in UAS.

2.5. UAS structure and processing

The UAS are composed by three main components: unmanned aerial vehicle, ground control station, and communication data link. Other components are part of the UAS structure such as navigation sensors, imaging sensors, and wireless systems.

Ground control station is defined as a stationary or transportable hardware and software devices to monitor and command the unmanned aircraft. Such equipment is very important for the UAS operation because if an eventual error occurs, it shall be sent to and see within the Ground Control Points (GCPs). For the GCPs to have a great operation, commanding devices are both navigation and orientation systems and the crew members need to command the UAS.

It is important to mention that UAS is autonomous system controlled via on-board autopilot and position information is provided using a global navigation and satellite system. The navigation and orientation system are composed by a tPVA (time, position, velocity, and altitude), which is defined during the mission planning. Besides that, during the mission planning other information are defined, such as, aircraft trajectory, waypoints, strips, flight speed, flying height, overlap between images, focal length, camera orientation, sensor configuration, triggering events, and flying directions.

Aiming to guarantee the UAS communication, several components are needed, such as, Global Navigation Satellite System (GNSS), Inertial Measurement Unit (IMU), baroaltimeter and compass. The GNSS is defined as a generic term for satellite navigation systems providing autonomous geo-spatial positioning with global coverage and IMU is defined as a self-contained system that has the goal of providing information about aircraft attitude at any given time. Aircraft attitude, in turn, is defined as a flight instrument that informs the pilot the aircraft orientation relative to the Earth’s horizon.

It is necessary to define the camera shutter speed, *i. e.*, the relationship between camera and lighting conditions. If the exposure time of the camera was too long, the imagery will be blurred or bright. But if the exposure time of the camera shutter is too short, the imagery will be dark to discriminate key-features of interest.

One very important step for UAS processing is camera calibration. Currently, the strategy used is based on the automatic detection and image measurement of tie points, known as Automatic Aerial Triangulation (AAT). During this mathematical process, a large number of tie points are generated with the goal of identifying multiple images.

Variations in the viewing geometry (roll, pitch, and yaw, as can be seen in Figure 6) can yield radiometric and geometric distortions in the final image mosaic. For reducing these distortions it is performed a process called the orthorectify.

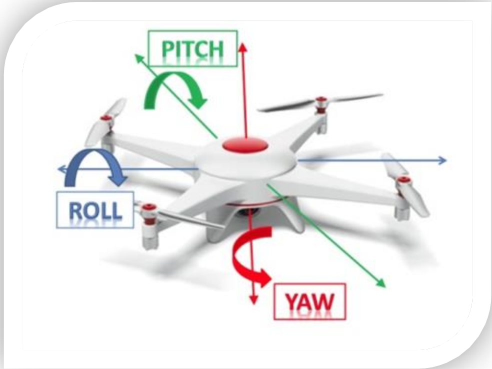

Figure 6: Representation of viewing geometry of UAS (roll, pitch and yaw).

With technological advances an algorithm was created, called ‘Structure from Motion (SfM), based on computer vision techniques, which made possible automatic tie points generation based on point detectors and descriptors of Scale Invariant Feature Transform (SIFT) type. The SIFT is a feature detection algorithm in computer vision used for detecting and describing local features in UAS images. In the final imagery, two main mapping are generated: orthophotos and Digital Surface Models (DSM). One of the advantages of the Structure from Motion is to produce Digital Surface Model (DSM), Digital Terrain Model (DTM) and mosaic in less time when compared to conventional photogrammetry process.

The DSM provides a detailed representation of the terrain surface, including elevations of objects (trees and buildings). The filtering of the dense point cloud is used to produce a DTM, which refers to a bare Earth model. The DTM is more useful than DSM because it removes the vegetation cover and buildings influence.

Differences in lighting image can be significant to UAS processing, for example, clouds are moving rapidly causing lighting differences in the imagery. This effect causes fails in ATT, resulting in error in the final images and causing a poor visual quality, with excessively dark or light in them.

Other issues caused by camera shortcomings or radiometric and geometric limitations are: cameras poorly calibrated, making difficult to convert brightness values to radiance; vignetting effects, which appear more frequently in edges than center image, but this effect can be reduced using a flat field process; chromatic aberration, causing a separation of colors at the edges of images (HAKALA et al. 2010).

The methods for reducing these issues are to remove photos that are blurred, saturated or overexposed; improve camera stabilization during flight or using a higher resolution fixed lens cameras (TURNER et al. 2012).

2.6. UAS applications

The uses and applications of the Unmanned Aerial Systems can be divided in six topics: military; agriculture and environmental; aerial monitoring in engineering; cultural heritage; local uses, and ecological processes (Table 5).

Topic	Uses
Agriculture and environmental application	- Forest fire monitoring; - Tectonic fractures; - Aggregate (sand and gravel) volumetrics; - Spatial and temporal variability in crops;
Military uses	- To detect lost people in difficult access situation; - Fire brigades in real time and crises management; - Decoys to fool enemy radars; - Provide broad area surveillance;
Aerial monitoring in engineering	- Characterize landslide on road ditches; - To monitor high and medium voltage lines; oil

	and gas pipe lines; roads and railways;
Cultural heritage	- Map archaeological villas; - Map ruins;
Local uses	- Analyze coastal erosion; - Land management, land consolidation and disaster monitoring; - Landform dynamics;
Ecological monitoring	- Animal and wildlife monitoring; - Bird and reptile monitoring; - Detect the presence and location of roe deer; - Phenological cycles; - Water status of vegetation; - Thermal properties of crop canopies; - Antarctic moss beds; - Analyze habitat hotspots.

Table 5: Description of UAS main application across six topics.

3. Study Area

The Espinhaço Range is the center of distribution of Brazilian rupestrian grassland or campo rupestre (Silveira et al. 2016). The diversity of species plants include more than 4000 species. The Espinhaço mountain chain, a relict of an ancient sea floor and deserts, is where most of the quartzite rupestrian grassland occurs (BARBOSA; SAD, 1973). In the Espinhaço, the Rupestrian Grassland is home to more than 6000 plant species with some families reaching up to 80 – 80% endemism (e.g. Giulietti et al. 1997; Rapini et al. 2008; Echternacht et al. 2011; Silveira et al. 2016).

Out study site, the Serra do Cipó, located in the southern portion of Espinhaço and with 200 km², less than 5% of the range, holds more than one third of this biodiversity (GIULIETTI, 1987). Image acquisition was done within the private conservation area belonging to *CEDRO Têxtil S.A.,* contained within the *Morro da Pedreira* Environmental Protection Area (Figure 7).

The dominant vegetation at Serra do Cipó, the rupestrian grasslands, is a component of the Cerrado floristic domain (Brazilian savanna). Rupestrian grasslands are found in altitudes above 900 meters, and are characterized by very high plant species richness and endemism (Silveira et al. 2016). This high biological diversity has been mostly explained by climatic oscillations in the Quaternary geological period (FERNANDES, 2018).

During the 18^{th} and 19^{th} centuries, the Espinhaço Range and, particularly Serra do Cipó, were impacted by human activities linked to gold and diamond exploration. With the decline of mineral deposits by the end of the 19^{th} century, the main economic activity of the region switched towards the tourism (RAPINI et al., 2008).

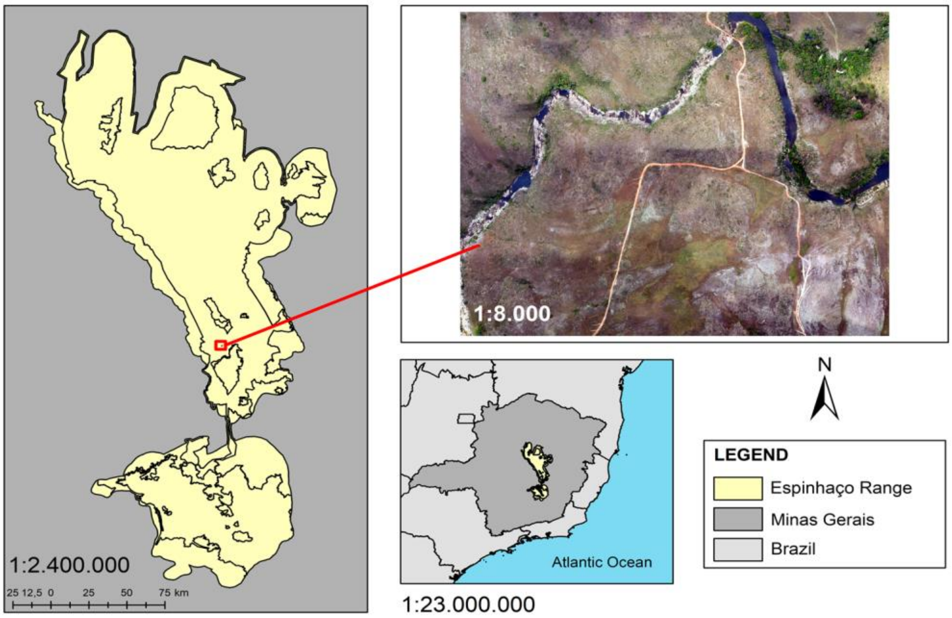

Figure 7: Location map of the study area, called “CEDRO”, in the Serra do Cipó, southern of the Espinhaço Range, where the imagery was performed, using UAS.

3.1. The Rupestrian Grassland, a heterogeneous ecosystem

The Rupestrian Grassland is an ancient ecosystem characterized by high herbaceous species richness, high endemism and unique species compositions (FERNANDES, 2016). The diversity of habitat types is also enormous in the Rupestrian Grassland. In quartzitic grasslands, sandy, stony and waterlogged grassland habitats, rocky outcrop, gallery forest, and relict hilltop forest patches, locally known as *capões de mata*, are the most common habitats (BENITES et al. 2007). The high biodiversity and endemism of the Rupestrian Grassland is influenced by latitudinal and altitudinal variations, land slope orientation, insularity and antiquity, which in synergy results in the creation of a great variety of soil types and microclimates where temperature, light, and humidity vary enormously (FERNANDES, 2016). These elements can be seen in Figure 8 and explained in Table 6.

The ancient age of the geological formation and a certain climatic stability, at least in the last few thousand years (BARBOSA et al. 2015), may have facilitated many evolutionary pathways leading to fine-tuned adaptations of the flora and fauna. It is likely that climatic stability may have promoted habitat predictability and allowed the synchronization of biotic and abiotic phenomena.

The complex topography of mountain environments may be responsible for the creation of a range of different microclimates that are of critical importance for species distribution (BROWN; LOMOLINO, 1998) as well as for the existence of true microrefugia, hence increasing biodiversity and strong site to site variation in species composition (BARBOSA at al. 2015). These mountain range separate the most diverse savanna of the world (the Cerrado) from the megadiverse Atlantic rain forest, being inserted between the 6th and the 4th biodiversity hotspots of the world, respectively.

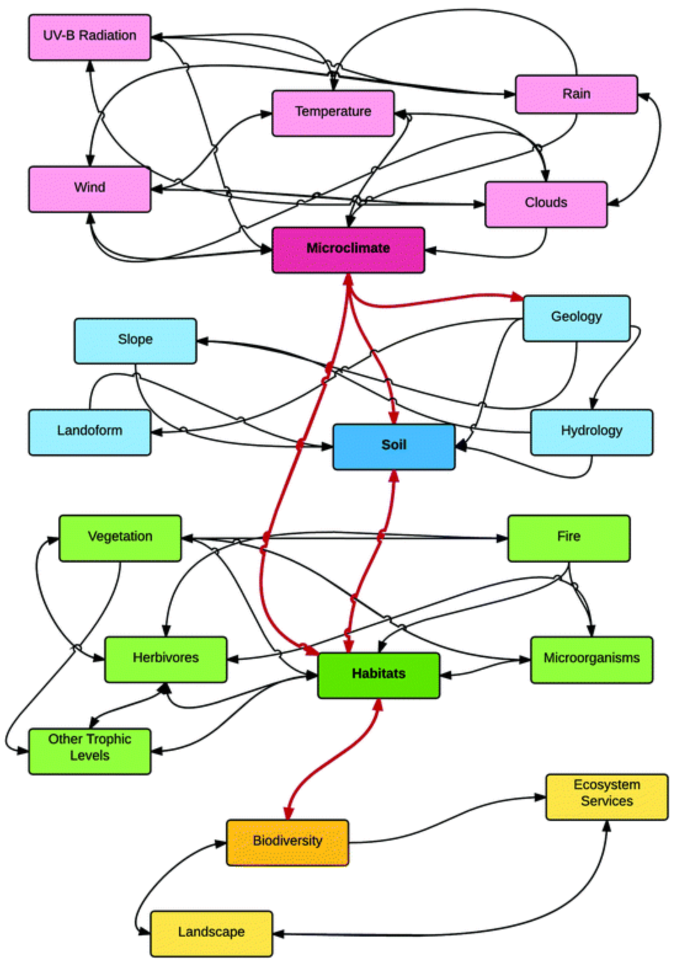

Figure 8: Factors influencing the biodiversity of the Rupestrian Grassland and, ultimately, its ecosystem services and landscape.

Square	Description
Pinkish squares	Climatic factors (UV-B Radiation, Temperature, Rain, Clouds, and Wind) which influence on biodiversity are very large and mostly driven by temperature and precipitation. The interaction of all factors creates a multitude of microclimates (darker pink).
Bluish squares	The geological origin of the terrain is also of major relevance to biodiversity. Mountains are shredded and eroded to form various landscapes and soils (darker blue square).
Greenish squares	Climatic variables act on the mother rock resulting in substrates of many textures and variable nutritional quality where plants colonize and persist. Such variables include the slope, landform, hydrology, site stability and soils, which influence the availability of heat, light, water, nutrients and the photosynthetic output of plants. Plants colonizing the different habitats are strongly influenced by climatic and soils factors, but also by fire, herbivores, microorganism, and other trophic levels.
Yellowish squares	The combination of the interaction of climate, geology, soils, vegetation and associated fauna in the variable landscape promote biodiversity and ecosystem services.
Red lines and arrows	Connect the major compartments (different colors), while connections among influencing factors are connected by black lines and

	arrows.

Table 6: Description and meaning of the factors influencing the biodiversity of the Rupestrian Grassland and, ultimately, its ecosystem services and landscape (Fig. 7).

3.2. Geological control

In Brazil, the Rupestrian Grassland Complex (RGC) grows on a range of geologies, including quartzite-sandstone (HARLEY; SIMMONS, 1986), granite-gneiss and itabirite, an iron-rich sedimentary rock (JACOBI; CARMO, 2011). Some researchers classified the RGC as 'vegetation refuges or relic vegetation types' floristically different from the dominant surrounding flora (VELOSO et al. 1991). Others proposed that such areas have acted as refuges during dry climate phases associated with major glaciations, as well as centers of recent speciation.

The RGC are associated with pre-Cambrian quartzites and metarenites, but it is important to mention that in different areas are found contrasting lithologies, for instance granites, gneisses, schists, syenites, metapelites, itabirites) and all of which representing the most resistant rocks in terms of chemical and physical conditions. The predominance of quartzite in RGC is explained by the following prerequisites:

1. Extreme oligotrophy;
2. Chemical resistance to weathering;
3. Physical resistance;
4. High mountain occurrence due to differential erosion;
5. Widespread distribution across the Brazilian Mobile Belts or the Ancient Brasiliano Orogenic Systems.

Through tectonically stable today, these areas are characterized as ancient mountain ranges former of greater development, during of tectonic collision between South American and

African Plates. The RGC are very old, residual cores of strongly weathered, folded, faulted and eroded landmasses. In terms of vegetation life forms, RGC is rich in geophytes (bulbous plants, a perennial plant, which in spring propagates from an underground organ), ericoids, proteoids and restiods.

3.3. Landforms and geomorphological control

Analyzing the Digital Elevation Model (DEM) of Brazil, it is clearly the relationship between the highlands above 1000 meters and the distribution of RGC (Figure 9). In these segments are common rock outcrops, which are related to stripping of the weathering mantle and exhumation of resistant rock cores, exposed by differential erosion (SCHAEFER, 2013). This process is variable in scale and depends on climate and paleoclimate conditions responsible for the balance between weathering, soil formation and erosion.

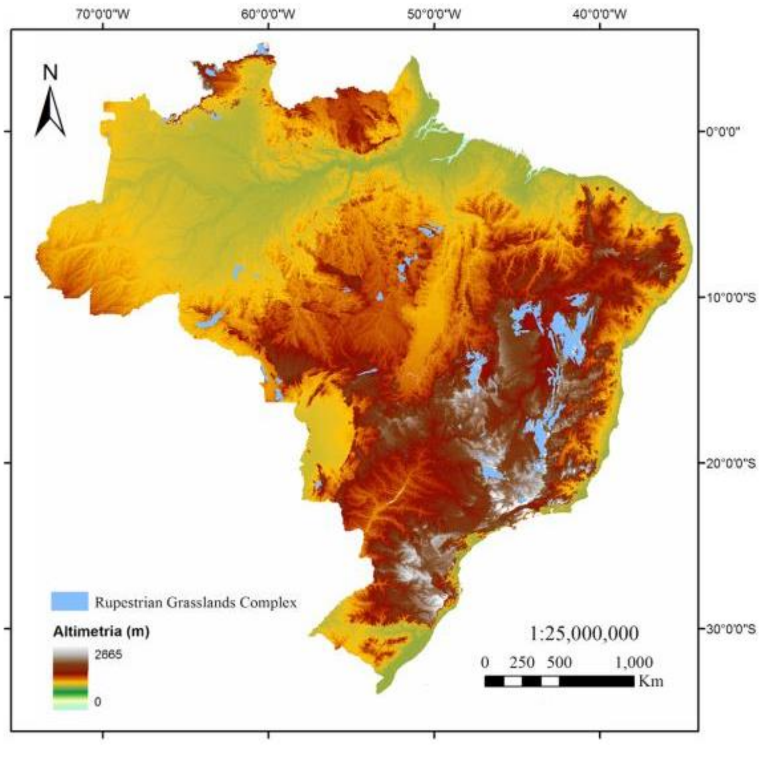

Figure 9: Digital Elevation Model (DEM) of Brazil and their relationship with Rupestrian Grassland Complex (RGC).

3.4. The human dimension in the Rupestrian Grassland

The Rupestrian Grassland has been threatened by a multitude of factors, for instance lack of ecological knowledge, mismanagement and lack of governance of the environment. These factors exposed have resulted in increased fire frequency, introduction of exotic invasive species, uncontrollable ecotourism, surface mining, road construction, real estate development, misinformed afforestation projects, and ongoing climate change (Fernandes et al. 2014; Veldman et al. 2015).

4. Materials and methods

4.1. Imagery and field data collection

Aerial photos were acquired using a 190 cm wingspan, 2.5 kg fixed wing UAV, built by G-Drones (http://www.g-drones.com.br/model) (Figure 10). The UAV was equipped with a CANON SX260 RGB camera, with 12 megapixels (6.2mm x 4.6mm, 4000 x 3000 pixels) of resolution and a focal length of 4.5 mm. The CHDK firmware (https://chdk.fandom.com) was installed on the camera, allowing it to run automated KAP UAV custom script, which enables automatic interval triggering of the camera during flight (https://chdk.fandom.com/wiki/KAP_UAV_Exposure_Control_Script). The UAV was equipped with Pixhawk V1 controlling board running the ArduPlane open source software (http://ardupilot.org/plane/), allowing for autonomous mission planning and execution using the Mission Planner software (http://ardupilot.org/planner/index.html#mission-planner-home). The flight lines, number of photos, and spatial resolution were automatically calculated based on the informed sensor size flight at 120 m above ground, and 80% overlap between consecutive flight lines. The mission covered a core 800 x 800 m square area (64ha), yielding footprints of with a nominal spatial resolution of 4 to 5 cm/pixels. The area was monitored at monthly intervals (from February 2016 to February 2017).

Figure 10: Fixed wing UAS, G-Plane Model used for photos acquisition equipped with a camera CANON SX260, sensor RGB of 12 megapixels of resolution.

The resulting aerial photos were mosaicked and orthorectified using the Pix4D Mapper 3.1 Educational software, using a proprietary implementation of Structure from Motion (SfM) algorithm. SfM is capable of extracting individuals reference points for alignment and automatic positioning of photos, generating a tridimensional point cloud, can then be used to generate a Digital Surface Model (DSM) and resulting orthomosaics (WESTOBY et al., 2012).

During July 2018, we also collected georeferenced ground trothing field points, according to predefined mapping classes (see Classification section). At each sampling point, the main vegetation/cover class was identified, and the location was logged using Garmin GPSMAP 64s (https://buy.garmin.com/en-US/US/p/140022/pn/010-01199-10) high-accuracy GPS receiver.

4.2. Orthomosaic registration

Due to the low accuracy of embedded camera GPS information, further manual co-registration was necessary to align the times series of orthomosaics. This step was performed on the ENVI 5.0 software. We chose as reference image the best image in the series in terms of brightness, and shading, as well as the closest alignment to Google Maps™ aerial imagery, which corresponded to the image acquired on 2016-09-25.

We then selected c.a. fifty ground control points (GCPs), between the reference image and each image to be co-registered, and then applied a second-order polynomial transformation with nearest neighbor pixel resampling, using a standardized 5 cm pixels grid. To estimate post-registration accuracy, we selected further GCPs between the reference image and a subsample of imaged dates, and then calculated horizontal, vertical and euclidean distance displacement between each image pair. The chosen dates for the validation process were 2016-02-23, 2016-05-22, 2016-08-16, 2016-11-30 and 2017-01-05.

4.3. Classification process

The classified images was 2016-09-25, 2017-01-05 and the stack with two images of the temporal series (2016-09-25 and 2017-01-05). The classification process was performed using the OBIA method. We first generated image objects using the Shepherd image segmentation algorithm implemented on “The Remote Sensing and GIS Software Library” (RSGISLIB), based on K-means clustering and accessible through the Python programming language (BUNTING et al., 2014). The K-means clustering algorithm is a learning algorithm that bunches a data through a number of clusters. The central idea this algorithm is define K centroids, one of each cluster. After, it is necessary use each point belonging to a given data set and associates it with the nearest centroid. Therefore, the initial association is completed. Through the global optimization method, some objects are redistributed to different clusters. This optimization is continued until the ideal assignment of objects to clusters is found (MACQUEEN, 1967).

This algorithm takes the following main parameters: NumClusters, MinPxls, DistThres, Sampling and KmMaxIter (Table 7). We tested ten different combinations of these parameters (Table 8) to determine the one that produced the best objects in terms of number of resulting objects vs. object homogeneity criteria. Assessment was done visually by inspecting the resulting objects overlaid on the base segmentation image.

Parameter	**Mean**
NumClusters	Number of K-means clusters – controls the general homogeneity and thus number of resulting objects. More clusters = more homogeneity, more objects.
MinPxls	Minimum size of the resulting objects.
DistThres	Distance threshold merging neighboring similar clusters.
Sampling	Number of pixels sampled for determining (K-means) clusters.
KmMaxIter	Maximum number of iterations for K-means clustering.

Table 7: Description of the parameters used in the RSGISLib software (Bunting et al. 2014) for segmenting UAV images from Serra do Cipó (Mg, Brazil) to support rupestrian grassland vegetation type classification.

Segmentation	NumClusters	MinPxls	DistThres	Sampling	KmMaxIter
1	20	100	10000	100	200
2	10	50	10000	500	100
3	5	500	5000	200	100
4	20	400	4000	300	200
5	30	30	5000	100	200
6	10	500	5000	100	200
7	30	400	5000	100	200
8	25	450	3000	100	200
9	15	450	5000	100	200
10	20	600	5000	100	200

Table 8: Tests of the segmentation process performed and their respective parameters (NumClusters, MinPxls, DistThres, Sampling and KmMaxIter).

The second step of the classification process was sample collection. This step is very important to improve quality classification. The training process was performed using a QGIS 2.18 and the samples were collected using georeferenced points acquired in fieldwork as part of the project FAPESP “"e-Phenology: Combining new technologies to monitor phenology from leaves to ecosystems". Our classification key was comprised of nine distinct spectral classes: ‘sandy grassland’, ‘stony grassland’, ‘wet grassland’, ‘rocky outcrop’, ‘cerrado scrubland’, and ‘riparian forest’ vegetation types, as well as ‘bare soil’, ‘bare rocks’ and ‘water body’ non-vegetation cover (Table 9). It is important to mention that 30% of the samples collected of each class were destined to validation and 70% to classification.

Spectral class	Characteristics	Number of samples collected	Photos
Bare soil	Roads and highways in general;	102	

			
Bare rocks	Bare rocks surfaces with complete absence of vegetation.	107	
Riparian forest	Forest formation along rivers and streams.	224	
Water body	Rivers and streams.	90	

Rocky outcrop	Rocky outcrops with significance and specific vegetation cover.	441	
Wet grassland	Herbaceous/shrub formations that occur in areas with groundwater upwelling or depressions that accumulate water during the rainy season.	150	
Cerrado scrubland	Herbaceous/shrub formations with sparse bushes, found on shallow soils of low fertility;	214	
Stony grassland	Herbaceous formations, with rare bushes, complete absence of trees and presence of stony/pebble substratum;	184	

Sandy grassland	Herbaceous formations growing on water and nutrient-poor sandy soils with high porosity, permeability, and erosion susceptibility.	292	

Table 9: Characteristics and number of samples collected in each spectral class.

With the goal of analyze the influence of the spatial resolution under the classification accuracy, the UAS original image, generated with spatial resolution of five centimeters, was aggregate progressively for spatial resolutions of 10, 25, 50 centimeters and one meter. This aggregation performed using the aggregate function available in the “raster” package of the programming language R. This function make possible the generation of raster’s with ticker resolution through rectangular aggregation of smaller pixels.

Image classification was also applied using the RSGISLIB library, which can access machine learning algorithms from the Sci-Kit Learn python (PEDREGOSA et al., 2011). The Random Forests classification algorithm was chosen, as it is a well-known and highly efficient classification ensemble learning algorithm. The Random Forest is a powerful machine learning tool that can be applied to identify the best performing features and build a robust classification model quickly. This algorithm produces an ensemble of decision trees and assigns the final class to each image object based on vote counting among the ensemble trees (BREIMAN, 2001). The main parameters of the Random Forest algorithm are *n-estimators* and *max-features*. The first refers to the number of decision trees generated by the classifier, and the second represent the maximum number of attributes considered by the algorithm from creating each node on each decision trees.

To assess the influence of spatial resolution on classification accuracy, the orthomosaics from 2016-09-25, originally generated with a spatial resolution of five centimeters, was progressively aggregated to the spatial resolution of 10, 25, 50 and 100 centimeters (1 meter), using the ‘aggregate’ function of the ‘raster’ package (Robert J. Hijmans (2016). Raster: Geographic Data Analysis and Modeling. R package version 2.5-8. https://CRAN.R-project.org/package=raster) of the programming language R (R Core Team (2017). R: A language and environment for statistical computing. R Foundation for Statistical Computing, Vienna, Austria. URL https://www.R-project.org/). Afterwards, the classification procedure was applied to each resulting image.

With the goal to evaluate the accuracy each of the classification was calculated the error matrix, general accuracy and Kappa index, through of 'rsacc' package developed to programming language R (https://github.com/EcoDyn/rsacc). The error matrix is a square matrix established in lines and columns, which the lines represents the data generated by classification and the columns represents the reference data (validation). The diagonal values refers to accuracy by class (correspondence between the classification and the observed), while the data out of the diagonal represent the percent of data classified wrong for each class (CONGALTON, 1991). The general accuracy is calculated through division between total sum of pixels of the main diagonal and total number of pixels of the error matrix. And the Kappa index is a concordance measure which considers the fact that even if classes were randomly assigned, some degree of agreement would be expected and, varies normally between 0 and 1.

5. Results and discussion

The results compilation could be divided in three sections: orthomosaic registration; segmentation and classification and influence of spatial resolution to species classification.

5.1. Orthomosaic registration

The complete alignment of the temporal series is important to obtaining concrete, effective and accurate results in the classification process. This step improved the quality and accuracy of images generated by UAS. For improving the accuracy of orthomosaic it is necessary to precise sensor position and orientation data, or several ground control points (GCPs) (TSAI; LIN, 2017). In following, we presented the registration results of five dates of temporal series: 23 of February of 2016; 22 of May of 2016; 16 of August of 2016; 30 of November of 2016 and 05 of January of 2016 (Figure 11 to 20).

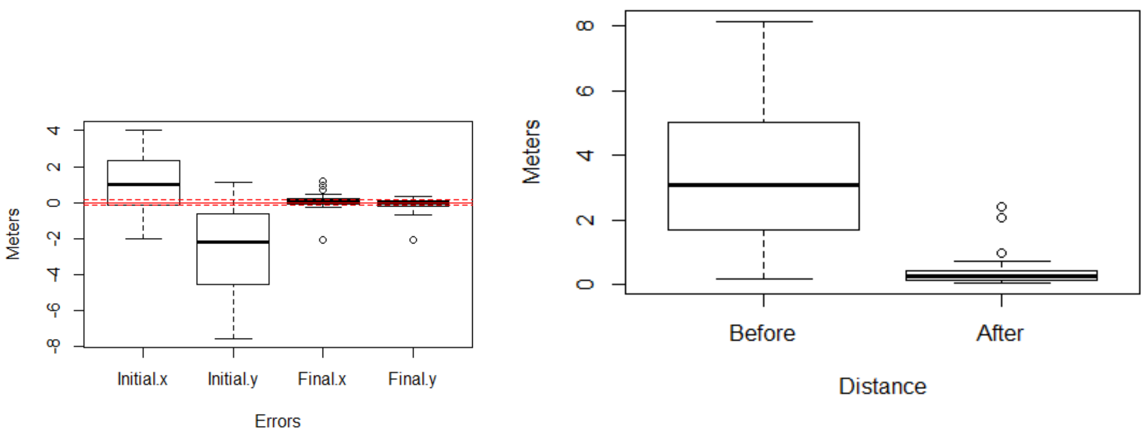

Figure 11: Horizontal, vertical and euclidean distance displacement to image of the 23 of February of 2016.

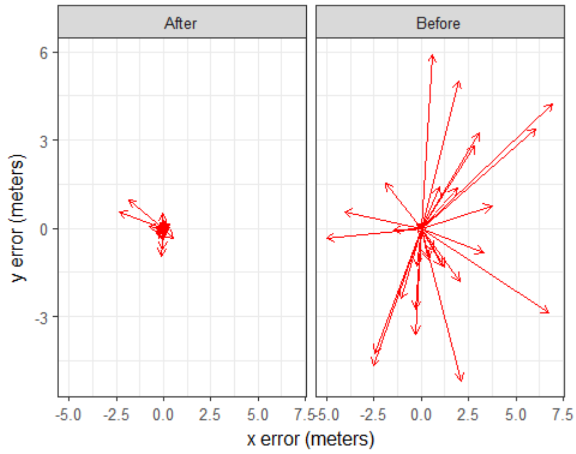

Figure 12: General accuracy of image registration to image of the 23 of February of 2016.

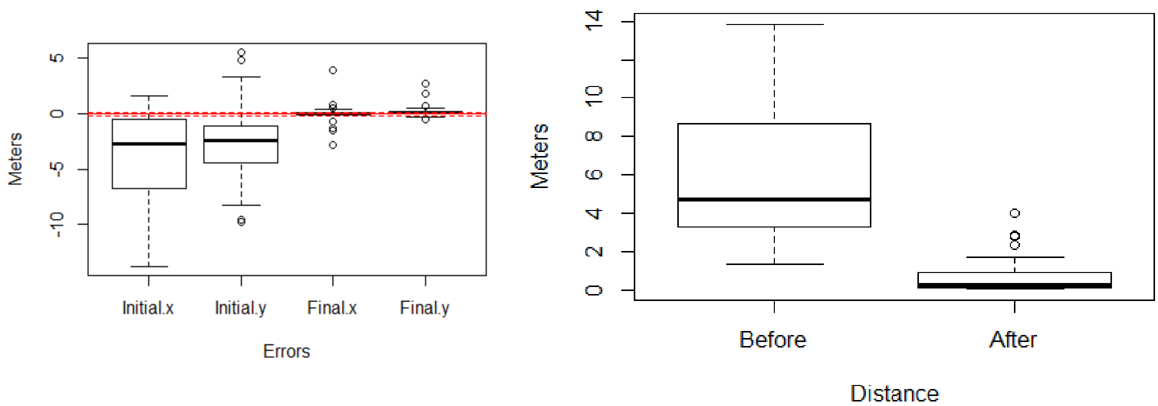

Figure 13: Horizontal, vertical and euclidean distance displacement to image of the 22 of May of 2016.

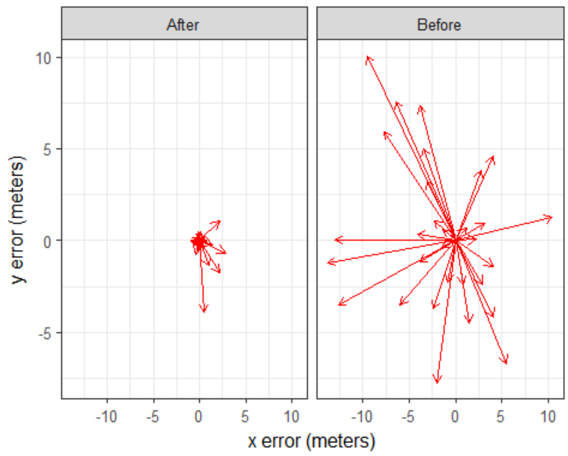

Figure 14: General accuracy of image registration to image of the 22 of May of 2016.

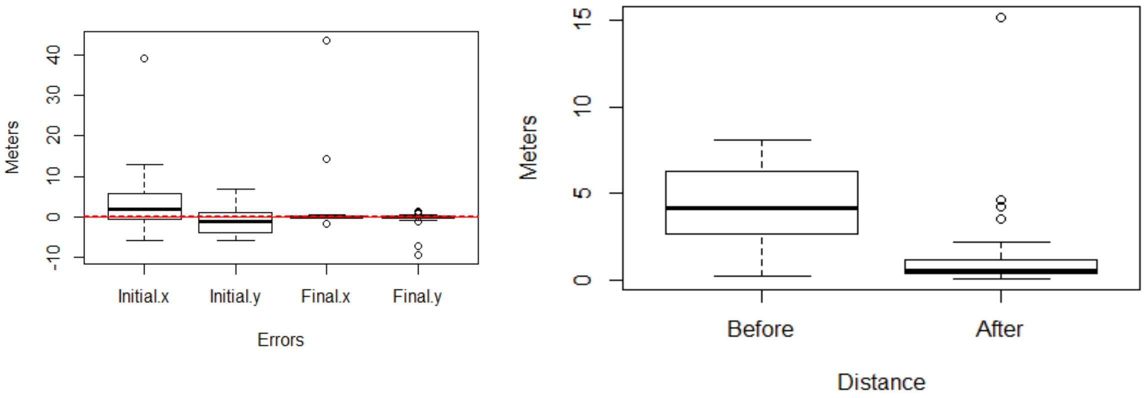

Figure 15: Horizontal, vertical and euclidean distance displacement to image of the 16 of August of 2016.

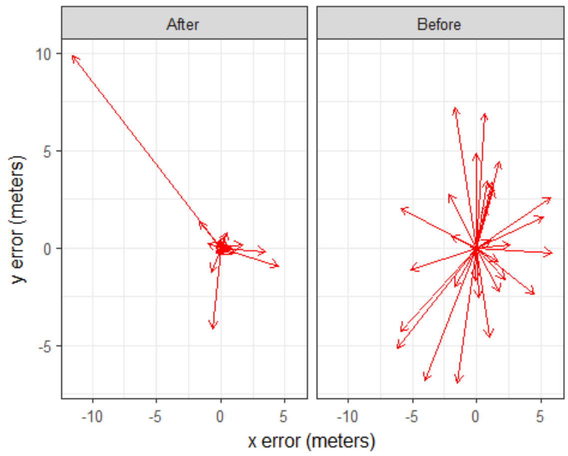

Figure 16: General accuracy of image registration to image of the 16 of August of 2016.

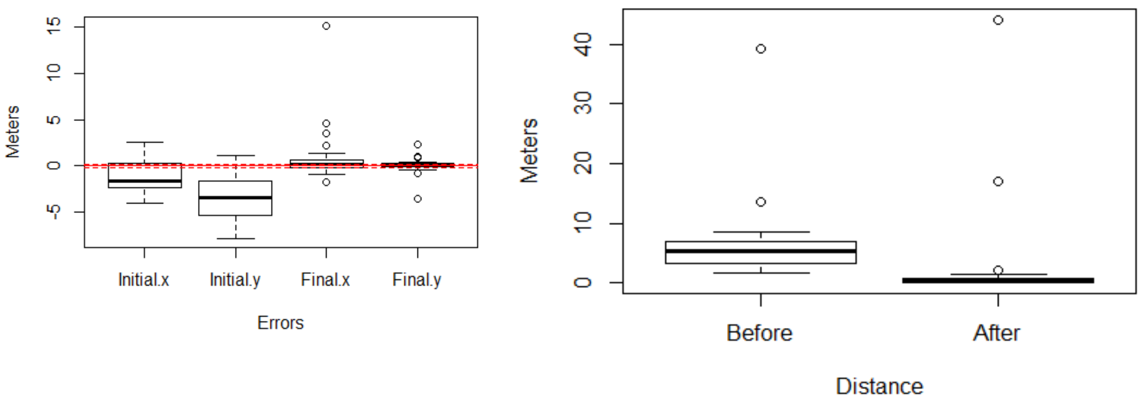

Figure 17: Horizontal, vertical and euclidean distance displacement to image of the 30 of November of 2016.

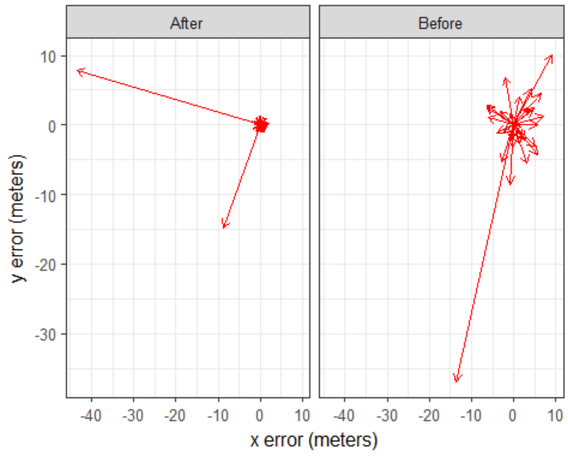

Figure 18: General accuracy of image registration to image of the 30 of November of 2016.

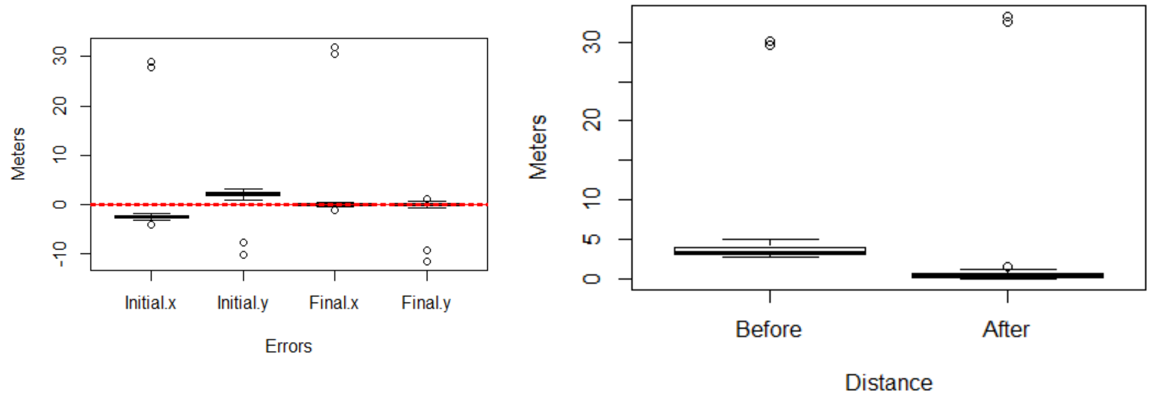

Figure 19: Horizontal, vertical and euclidean distance displacement to image of the 05 of January of 2017.

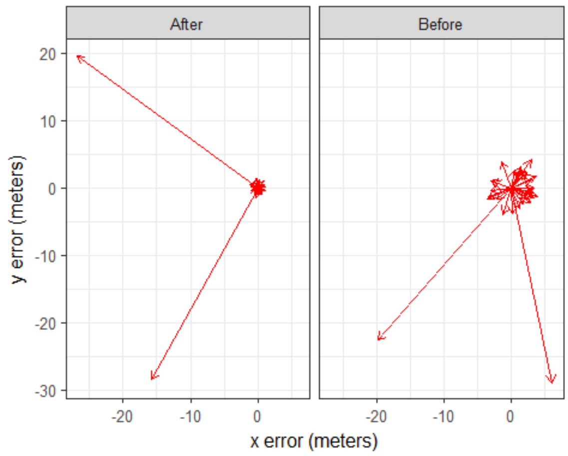

Figure 20: General accuracy of image registration to image of the 05 of January of 2017.

In general, the horizontal, vertical and euclidean distance displacement reduced on average from 2 – 10 meters before the registration process to 0 – 2 meters after the registration process. These results can be seen in Table 10.

Date	Horizontal Error Initial x (Before)	Vertical Error Initial y (Before)	Horizontal Error Final x (After)	Vertical Error Final y (After)	Euclidean distance error Before	Euclidean distance error After
02/23/2016	1.0518	-2.5983	0.08496	-0.1156	3.4133	0.44185
05/22/2016	-3.6554	-2.589	-0.04921	0.24062	6.188	0.72201
08/16/2016	-1.1742	-3.571	0.8573	0.05	4.3193	1.47680
11/30/2016	3.3064	-0.8325	1.91457	-0.525017	6.361	2.47051
01/05/2017	-0.5232	1.433	2.01524	-0.65870	5.181	2.5736

Table 10: Summary of the results obtaining with the validation process: horizontal error – initial x (before of the registration process); vertical error – initial y (before); horizontal error – final x (after of the registration process); vertical error – final y (after); euclidean distance error (before) and euclidean distance error (after) of each date chosen for the validation. The values were expressed based on mean of errors and in meters.

5.2. Segmentation and classification

Among all the segmentation tests, it was possible to conclude that one of the best suits patterns and homogeneity criteria was ten segmentation, according to enumerated in Table 8 (Section 4.3. Classification process). This segmentation produced results that covered properly the homogeneity areas of the image. We analyzed what was the better parameters combination using the visual criteria, as illustrated in the image of the Figure 21:

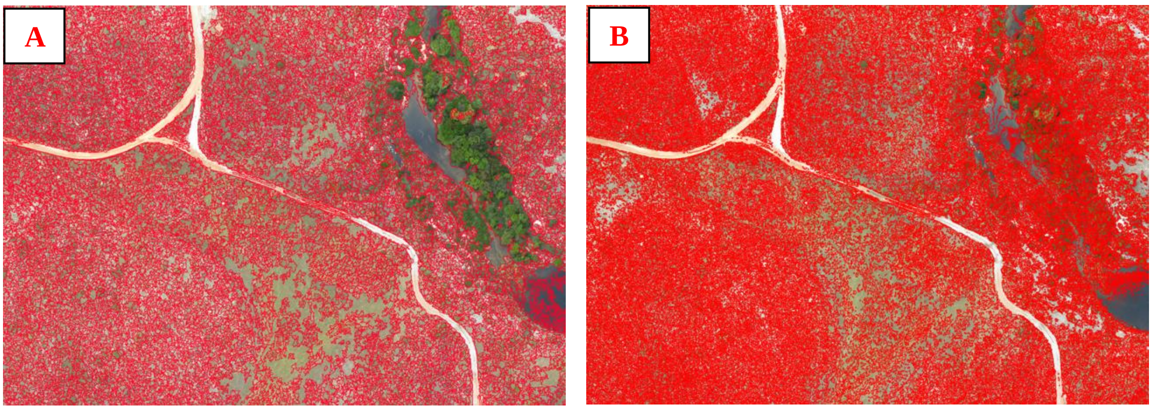

Figure 21: The better result of segmentation process (NumClusters = 20 and MinPxls = 600) (A) and the worst result of segmentation process (NumClusters = 10 and MinPxls = 50) (B).

According described in Table 11, strategies was realized with the goal of analyze the application of OBIA method in image with high spatial resolution, between them the different numbers of decision trees, classification with a unique image, classification with stack and different combinations of segmentation parameters. It is possible conclude that 200 numbers of decision trees and only two attributes (color and form) did not enough to classify the rupestrian grassland according to the reality of the heterogeneous environment. Other relevant information is that the stack process with the image dated to September 25th 2016 and dated to January 05th 2017 was interesting to improve the general accuracy and KAPPA index. Finally, in this process were used 500 numbers of decision trees and three attributes: color, texture and form. This classification received 0.96 to general accuracy and 0.95 to KAPPA Index.

Date of the orthomosaic classified	K-means clustering *NumClusters | MinPxls*	Random Forest *N - estimators*	Results General Accuracy | KAPPA
1 – 09/25/2016	5 | 500	10	0,6919 | 0,6228
2 – 09/25/2016	5 | 500	200	0,7043 | 0,6382
3 – *Stack*	5 | 500	500	0,8599 | 0,8344
4 – *Stack*	20 | 600	500	0,9619 | 0,9545

Table 11: Results of the classification tests realized in the research

In the stack process is important to use one image of the dry season and one image of the wet season (Figure 22 and Table 12). In the tropical climate, the dry season is characterized by low precipitation and temperatures, on the other hand, the wet season is characterized by high precipitation and temperatures. According to National Agency of Water (*Agência Nacional de Águas*, in Portuguese), the winter presents a rainfall regime around 8 mm, while the summer presents a rainfall regime around 232 mm. These processes have an influence on phytophysionomies behavior. During in dry season, the species of plants tend to enter the wilting process because of the water deficit, causing a differentiation in color composition of the orthophoto (the species staying more yellowish), and in wet season the species of the plants will enter it is flowering process, changing the color pattern of the plants, which is visible in orthophotos (the species staying more greenish). Because of these processes, the use of the stack is essential for understanding and capturing different phenological stages.

Capturing different phenological stages and different behavior of the phytophysionomies help the algorithm to classify properly the spectral classes present in rupestrian grassland of the Serra do Cipó – MG, and thus promote a classification consistent with the reality. This process of improvement of the segmentation and classification through the OBIA method with the use of high-level image details (UAS) is very important for understanding and studying these environments, which, currently, suffer a lot of human activities that increasingly deforest and destroys such ecosystems.

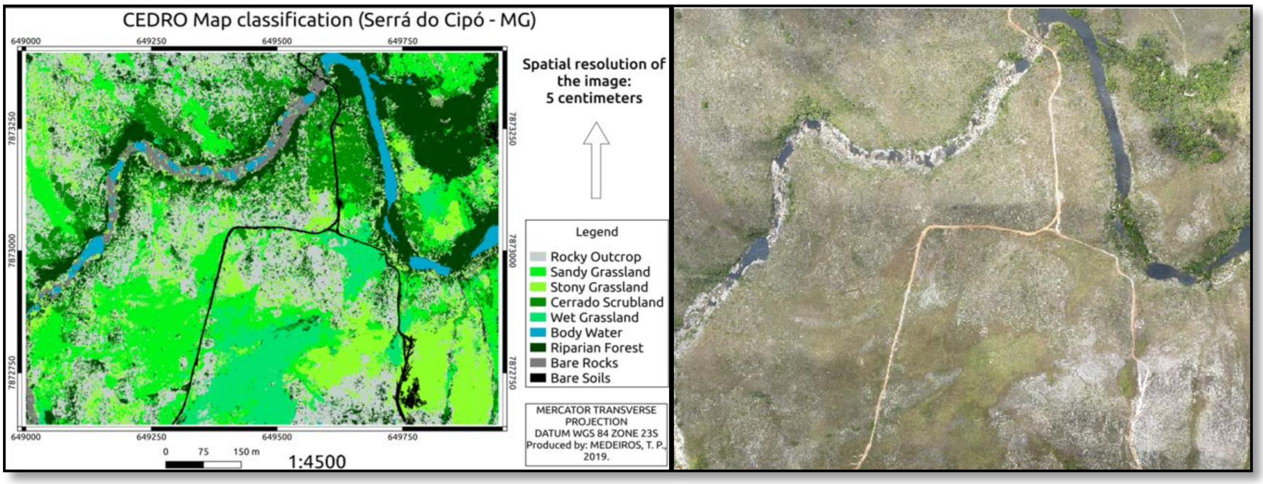

Figure 22: Classification using the stack with two images of the series temporal: image dated to September 25th 2016 and image dated to January 05th 2017.

	Rocky Outcrop	Sandy Grassland	Stony Grassland	Cerrado Scrubland	Wet Grassland	Body Water	Riparian Forest	Bare Rocks	Bare Soils
Rocky Outcrop	**10,32**	0,05	0,0009	0,0003	0,002	0	0,008	0	0
Sandy Grassland	0,009	**18,69**	0,014	0,32	0	0	0,046	0	0
Stony Grassland	0	0,07	**16,71**	0,057	0	0	0	0	0
Cerrado Scrubland	0,001	0,015	0,37	**9,13**	0	0	0,009	0	0
Wet Grassland	0,01	**1,46**	0	0,086	**11,11**	0,083	0,04	0	0
Body Water	0,11	0	0	0	0	**5,29**	0,11	0,046	0
Riparian Forest	0	0	0	0,01	0	0,18	**28,61**	0,34	0
Bare Rocks	0	0	0	0,043	0	0	0	**2,39**	0
Bare Soils	0	0	0,53	0,01	0,076	0	0	0,012	**2,27**

Table 12: Error matrix for the stack classification realized with two images of the temporal series (in %).

5.3. Spatial resolution to species classification results

The aggregation for thicker spatial resolutions (10, 25, 50 and 100 centimeters) caused a reduction in the heterogeneity of the original image. However, in thinner resolutions we have the reduction in features homogeneity. The calculation of the standard deviation for each classification and their respective spatial resolution is an important indicator of the decrease or increase of the homogeneity in the image, that is, higher standard deviation can indicate high data variability and, consequently, more heterogeneity, and these can be seen in the classification of spatial resolution of 5 centimeters and 10 centimeters. However, the lower standard deviation can indicate low data variability and, consequently, more homogeneity, and these can be seen in the classification of the spatial resolution of 50 centimeters and one meter (Figure 23).

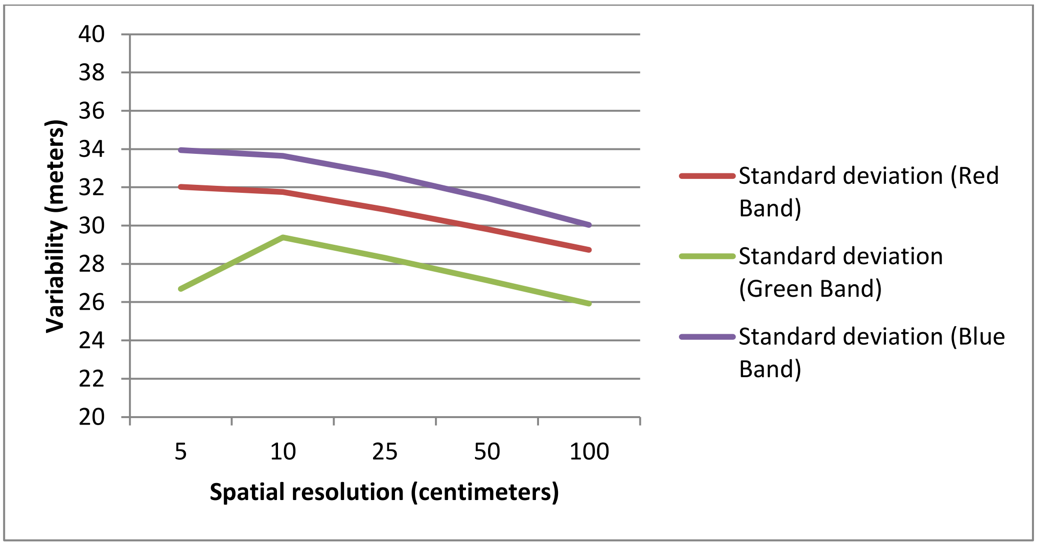

Figure 23: Standard deviation of each spectral band and of each spatial resolution.

After of performing the validation process, it is possible to conclude that the classification that presents the better result is the one with resolution of 25 centimeters, which received the values of 0.78 for general accuracy and 0.73 for KAPPA Index. On the other hand, the worst result was performed by classification of 5 centimeters of spatial resolution and received the values of 0.70 for general accuracy and 0.64 for KAPPA Index. This result could be associated with the difficulty of the OBIA method to identify the spectral vegetation classes in front of the heterogeneity in images with high resolutions. These results can be seen in Figure 24.

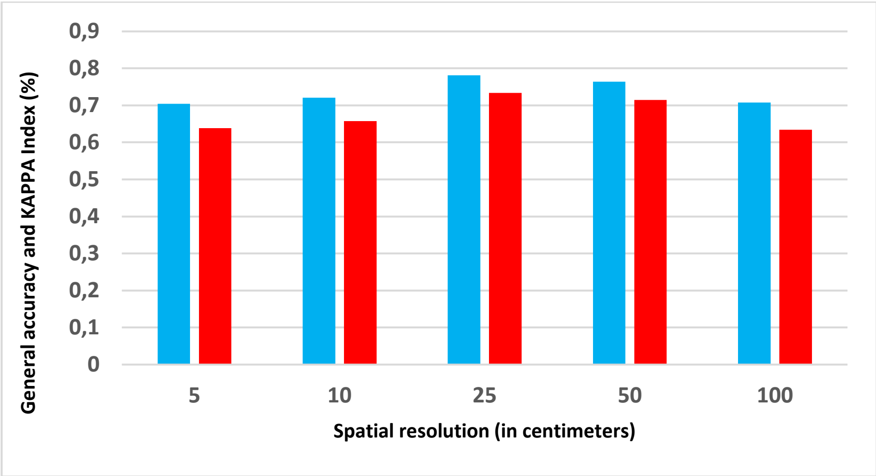

Figure 24: Results of the classification: general accuracy and KAPPA Index of each spatial resolution.

Another important point to mention is that in thinner resolutions, 5 and 10 centimeters, the confusion patterns of the features are high, decreasing the accuracy rates and KAPPA Index (Figure 25). When the heterogeneity is lost, the confusion patterns of the features have a decrease and, consequently, the accuracy rates and KAPPA Index increases (Figure 26). It is possible to visualize this confusion patterns in some cases, for instance, between the spectral classes 'rocky outcrop', 'sandy grassland' and 'riparian forest' and between the spectral classes 'riparian forest' and 'cerrado scrubland'. This confusion can be explained by similar coloration between the physiognomies and the textural similarity of both. These confusions can be seen in Table 13 and 14.

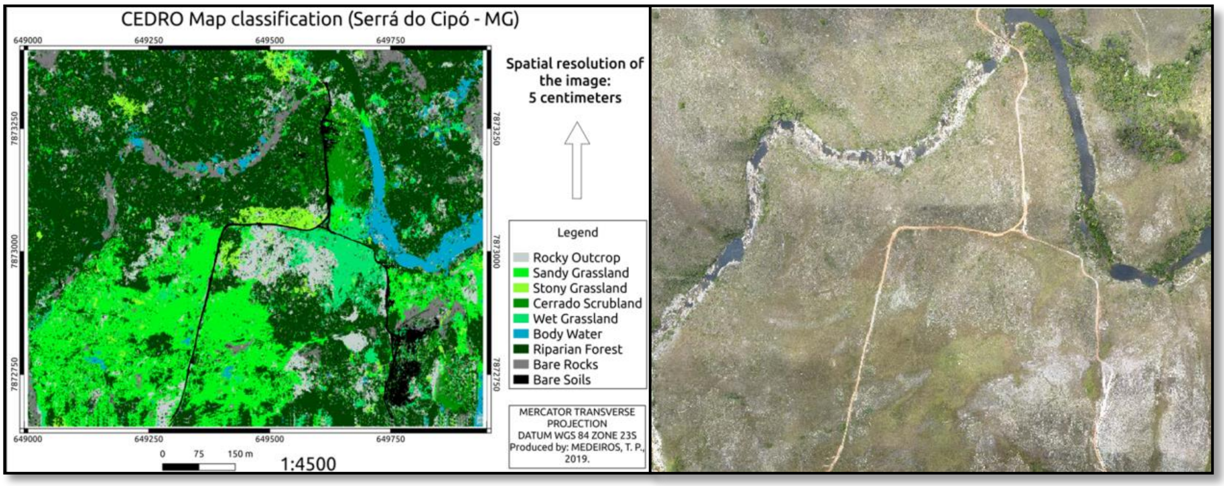

Figure 25: The worst result of the classification: orthophotos of 5 centimeters of spatial resolution.

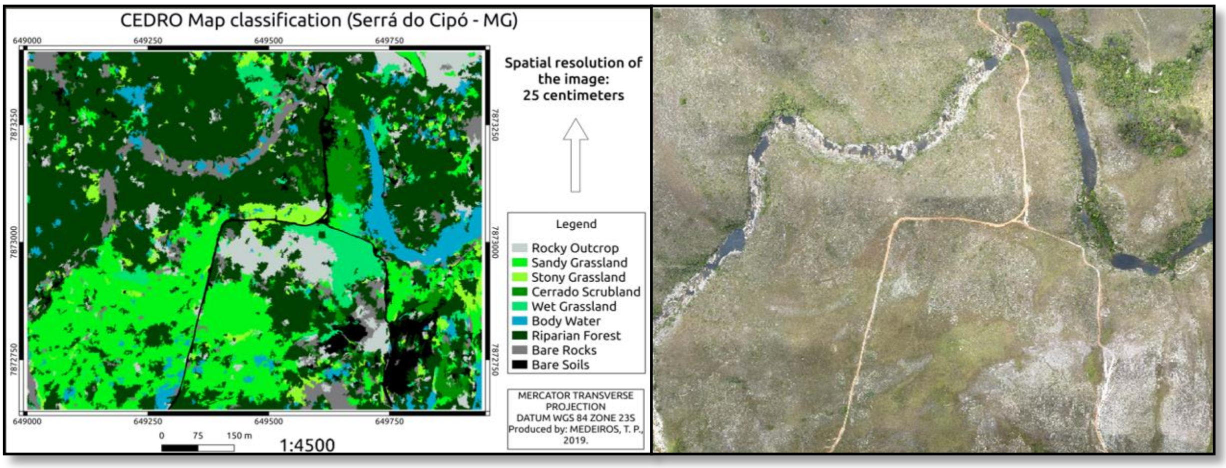

Figure 26: The better result of the classification: orthophotos of 25 centimeters of spatial resolution.

	Rocky Outcrop	Sandy Grassland	Stony Grassland	Cerrado Scrubland	Wet Grassland	Body Water	Riparian Forest	Bare Rocks	Bare Soils
Rocky Outcrop	**5,99**	0,27	0,38	0,15	0,08	0	1,41	0,03	0,04
Sandy Grassland	1,87	**20,97**	0,31	0,02	0,36	0,01	1,59	0,17	0,01
Stony Grassland	0,19	0,01	**0,6**	0,31	0,03	0	0,25	0	0
Cerrado Scrubland	0,41	0,14	0,13	**5,07**	0,07	0	1,09	0,11	0
Wet Grassland	0,53	0,66	0,07	0,53	**7,47**	0,19	1,09	0,14	0
Body Water	0,04	0,01	0	0	0	**2,25**	6,3	0,06	0
Riparian Forest	1,65	0,53	0,37	1,3	0,31	3,43	**18,51**	1,14	0
Bare Rocks	0,21	0,11	0,04	0,21	1,65	0	1,85	**4,4**	0,1
Bare Soils	0	0	0,01	0,41	0	0	0,01	0,02	**1,94**

Table 13: Error matrix for classification of 5 centimeters of spatial resolution (in %).

	Rocky Outcrop	Sandy Grassland	Stony Grassland	Cerrado Scrubland	Wet Grassland	Body Water	Riparian Forest	Bare Rocks	Bare Soils
Rocky Outcrop	**8,14**	0,47	0,06	0	0	0	2,81	0,24	0
Sandy Grassland	1,58	**21,92**	0,52	0	0,42	0	0,7	0	0
Stony Grassland	0	0	**1,21**	0,28	0	0	1,17	0	0
Cerrado Scrubland	0	0,04	0	**5,66**	0,07	0	1,28	0	0
Wet Grassland	0,08	0,62	0	0,03	**8,14**	0,19	0,29	0	0
Body Water	0,05	0	0	0	0	**2,56**	6,91	0	0
Riparian Forest	0,85	0	0,17	1,57	0	3,21	**18,43**	0,49	0
Bare Rocks	0	0	0	0	0	0,01	0,54	**5,47**	0,11
Bare Soils	0	0	0	0,62	0	0	0,01	0	**2,97**

Table 14: Error matrix for classification of 25 centimeters of spatial resolution (in %).

6. Conclusions

Monitoring and understanding a heterogeneous environment, such as rupestrian grassland of the Serra do Cipó – MG, area with high endemicity of herbaceous species, very important to ecosystem of the Espinhaço Range, suffer with the expansion of monoculture of pines and eucalyptus, and that, therefore, the existing mosaic of species runs the risk of extinction, it is very important so that we can preserve this biodiversity and guarantee the permanence of the mosaic of species.

The use of the UAS is essential, currently, for monitoring such an ecosystem, because this technological tool presents a lot of benefits, for instance: high flexibility in temporal resolution, high spatial resolution, low-cost. Meanwhile, these types of equipment present a few challenges in the classification of elements of the Earth's surface and, for this, the work of method improvement is necessary and needs more studies.

It was possible to analyze that high heterogeneity of the surface elements in images with five centimeters of spatial resolution produced a lot of confusion in the algorithm, but these confusions can be reduced using the stack with two or more images of the temporal series. The stack helps the algorithm understanding the vegetation patterns and proposed better classification results.

In the future, it is interesting to apply this methodology for other regions of the Serra do Cipó or for other heterogeneous environment and to compare the areas with other abiotic factors (geomorphology, soils, geology, climate, and others). This comparison can promote a more complete study and a deeper understanding of the potentialities and vulnerabilities of such environments.

7. References

ANDERSON, K.; GASTON, K. J. Lightweight unmanned aerial vehicles will revolutionize spatial ecology. Frontiers in Ecology and the Environment, 2013.

BARBOSA, A. L. M.; SAD, J. H. G. Tectonic control of sedimentation and trace-element distribution in iron ores in central Minas Gerais (Brazil). In: Proceedings of kiev symposium: Genesis of Precambrian iron and manganese deposits, UNESCO, p. 125 – 131, 1973.

BARBOSA, A. L. M. et al. A relict species restricted to a quartzitic mountain in tropical America: an example of microrefugium? Acta Bot Bras, v. 29, p. 299 – 309, 2015.

BENITES, V. M. et al. Soil associated with rock outcrops in the Brazilian mountain ranges Mantiqueira and Espinhaço. Rev Bras Bot, v. 30, p. 569 – 577, 2007.

BLASCHKE, T. Object based image analysis for remote sensing. ISPRS Journal of Photogrammetry and Remote Sensing, v. 65, p. 2–16, 2010.

BREIMAN, L. Random Forests. University of California, Berkeley, 2001.

BROWN, J. H.; LOMOLINO, M. V. Biogeography. Sinauer, Sunderland, 1998.

BUNTING, P. et al. The Remote Sensing and GIS Software Library (RSGISLib). Computers & Geosciences, v. 62, p. 216-226, 2014.

COLOMINA, I.; MOLINA, P. Unmanned aerial systems for photogrammetry and remote sensing: A review. ISPRS Journal of Photogrammetry and Remote Sensing, v. 92, p. 79–97, 2014.

CONGALTON, R. G. A review of assessing the accuracy of classifications of remotely sensed data. Remote Sensing Environment, v. 37, p. 35 – 46, 1991.

ECHTERNACH, L. et al. Areas of endemism in the Espinhaço range in Minas Gerais, Brazil. Flora, v. 206, p. 782 – 791, 2011.

EVERAERTS, J. Newplatforms – unconventional platforms (Unmanned Aircraft Systems) for remote sensing. Technical Report 56. European Spatial Data Research (EuroSDR). 2009.

FERNANDES, G. W. et al. Challenges for the conservation of vanishing megadiverse rupestrian grassland. National Conservation, v. 12, p. 162 – 165, 2014.

FERNANDES, G. W. Ecology and Conservation of Mountaintop grasslands in Brazil. Cham: Springer International Publishing, 2016.

FERNANDES, G. W. et al. The deadly route to collapse and the uncertain fate of Brazilian rupestrian grasslands. Biodiversity and Conservation. Online first: https://doi.org/10.1007/s10531-018-1556-4, 2018.

GIULIETTI, A. M. et al. Flora da Serra do Cipó, Minas Gerais: Caracterização e lista das espécies. Boletim de Botânica da Universidade de São Paulo, v. 9, n. May, p. 1–151, 1987.

GIULIETTI, A.M.; PIRANI, J.R.; HARLEY, R.M. Espinhaço range region. Eastern Brazil. Centers of plant diversity. A guide and strategies for the conservation, v. 3, p. 397 – 404, 1997.

GOULD, W. Remote sensing of vegetation, plant species richness, and regional biodiversity hotspots. Ecological Applications, v. 10, p. 1861 – 1870, 2000.

HAKALA, T.; et al. Acquisition of bidirectional reflectance factor dataset using a micro unmanned aerial Vehicle and a consumer camera. Remote Sensing, v. 2, n° 3, p. 819 – 932, 2010.

HARDIN, P. J.; JENSEN, J. R. Small-scale unmanned aerial vehicles in environmental remote sensing: challenges and opportunities. GIScience Remote Sensing, v. 48, p. 99 – 111, 2011.

HARLEY, R. M.; SIMMONS, N. A. Florula of Mucugê, Chapada Diamantina – Bahia, Brazil. Royal Botanical Garden, 1986.

JACOBI, C. M.; CARMO, F. F. Life-forms, pollination and seed dispersal syndromes in plant communities on ironstone outcrops. Acta Bot Bras, v. 25, p. 395 – 412, 2011.

JENSEN, J. R. Remote sensing of the Environment: an earth resource perspective. Brigham Young University: Prentice-Hall, 2nd edition, 2006.

KOSTRZEWA, J. et al. Infrared microsensor payload for miniature unmanned aerial vehicles. Unattended Ground Sensor Technologies and Applications, v. 265, 2003.

LALIBERTE, A. S.; RANGO, A. Image processing and classification procedures for analysis of sub-decimeter imagery acquired with an unmanned aircraft over arid rangelands. GIScience & Remote Sensing, v. 48, n° 1, p. 4 – 23, 2011.

LU, B.; HE, Y. Species classification using Unmanned Aerial Vehicle (UAV) – acquired high spatial imagery in a heterogeneous grassland. ISPRS Journal of Photogrammetry and Remote Sensing, v. 128, p. 73-85, 2017.

MACQUEEN, J. Some methods for classification and analysis of multivariate observations. Western Management Science Institute, v. 233, n°, 75, 1967.

MACKENZIE, R. Environmental and Earth science using next generation aerial platforms. 2009.

MORELLATO, L. P. C.; SILVEIRA, F. A. O. Plant file on campo rupestre: new lessons from an ancient biodiversity hotspot. Flora, v. 238, p. 1-10, 2018.

NEX, F.; REMONDINO, F. UAV for 3D mapping application: a review. Applied Geomatics, v. 6, n° 1, p. 1 – 15, 2013.

PEDREGOSA *et al*. Scikit-learn: Machine Learning in Python. JMLR 12, pp. 2825-2830, 2011.

RAPINI, A. *et al*. A flora dos campos rupestres da Cadeia do Espinhaço. Megadiversidade, v. 4, p. 16–24, 2008.

REMY, M. et al. The first UAV based P and X band interferometric SAR system. IEEE, Germany, p. 5041 – 5044, 2012.

ROCHA, N. M. B.; CARSTENSEN, D. W.; FERNANDEZ, G. W.; MORELLATO, L. P. C. Phenology patterns across a rupestrian grassland altitudinal gradient. Ecology and conservation of mountain top grassland in Brazil. Springer, New York, 2016.

RUFINO, G.; MOCCIA, A. Integrated VIS-NIR Hyperspectral / Thermal-IR Electro-optical payload system for a mini-UAV. American Institute of Aeronautics and Astronautics, Arlington, UAS, p. 647 – 664, 2005.

SCHAEFER, C. E. G. R. Bases físicas da paisagem brasileira: estrutura geológica, relevo e solos. In: Tópicos em ciência do solo. Sociedade Brasileira de Ciência do Solo, Viçosa, p. 1 – 69, 2013.

SILVEIRA, F. A. O. et al. Ecology and evolution of the endangered campo rupestre: a neglected biodiversity conservation priority. Plant and Soil, v. 403, p. 129-152, 2016.

TSAI, C. H.; LIN, Y. C. An accelerated image matching technique for UAV orthoimage registration. ISPRS Journal of Photogrammetry and Remote Sensing, v. 128, p. 130 – 145, 2017.

TURNER, D.; LUCIEER, A.; WATSON, C. An automated technique for generating georectified mosaics from ultrahigh resolution unmanned aerial vehicle (UAV) imagery based on Structure from Motion (SfM) point clouds. Remote Sensing, v. 4, n° 5, p. 1392 – 1410, 2012.

VAN-BLYENBURGH, P. Remotely Piloted Aircraft Systems: the global perspective. RPAS Yearbook. Technical Report. UVS International. Paris, France. 2013.

VELDMAN, J. W. et al. Toward an old-growth concept for grasslands, savannas, and woodlands. Frontiers Ecological Environment, v. 13, p. 154 – 162, 2015.

VELOSO, H. P. et al. Classificação da vegetação brasileira, adaptada a um sistema universal. Instituto Brasileiro de Geografia e Estatística, Rio de Janeiro, 1991.

WESTOBY, M. J.; BRASINGTON, J.; GLASSER, N. F.; HAMBREY, M. J.; REYNOLDS, J. M. ‘Structure from Motion’ photogrammetry: A low cost, effective tool for geoscience applications. Geomorphology, v. 179, p. 300 – 314, 2012.

WATTS, A. C.; AMBROSIA, V. G.; HINKLEY, E. A. Unmanned Aircraft Systems in Remote Sensing and Scientific Research: classification and considerations of use. Remote Sensing Journal, v. 4, p. 1671 – 1692, 2012.

WESTER-EBBINGHAUS, W. Aerial photography by radio controlled model helicopter. The Radiometric Record, v. 10, p. 85 – 92, 1980.

WHITEHEAD, K.; HUGENHOLTZ, C. H. Remote sensing of the environment with small Unmanned Aircraft System (UASs), part 1: a review of progress and challenges. NRC Research Press, v. 2, p. 69-85, 2014.

XIE, F. et al. Study on construction of 3D building based on UAV images. ISPRS Journal of Photogrammetry and Remote Sensing, p. 469 – 473, 2012.